Published by :
http://www.ijert.org

International Journal of Engineering Research & Technology (IJERT)
ISSN: 2278-0181
Vol. 10 Issue 08, August-2021

Design and Simulation of MEMS based Capacitive Accelerometers for Crash Detection and Airbag Deployment in Automobile

Mr. Kiran Teradal, Mr. Mukul Karwa, Mr. Nikhil N Kumar, Mr. Raihan Mohammed R
PES Institute of Technology, Hosur Road,
Bangalore 560100

***Abstract*:- This paper focuses on design and analysis of MEMS based accelerometer to detect accidents and for the deployment of airbags. In the case of a car accident, where there are sudden and strong accelerations, it is necessary to measure as fast as possible their intensity and direction with good accuracy and precision, aiming to reduce the injuries severity to passengers. With the continuous advancements in Micro Electro Mechanical Systems (MEMS) fabrication technology, inertial sensors like accelerometers and gyroscopes can be designed and manufactured with smaller footprint and lower power consumption. Capacitive accelerometers are the most popular and highly researched due to several advantages like high sensitivity, low noise, low temperature sensitivity, linearity, and small footprint. When sudden displacement occurs due to impact the comb gets shock loads or forces and that movement is observed by differential capacitance concept with dielectric as air. The simulations will be carried out on COMSOL while the design will be carried out on COMSOL, the actual theoretical calculation and the simulations are compared in order to get accurate results. The capacitance output obtained is carried to the electronic control unit which sends the impulse signal to air bag system and deployment of air bags takes place.**

INTRODUCTION:

Automotive is one of the most emerging area since ages and is constantly under developments. These developments in technology and these advancements are not without responsibilities to assure that the end user is safe and satisfied. The industries' primary concerns are improving the performance, safety, and comfort aspects which have become evident over the years with introduction of highly improved standards with every iteration. Passenger safety is a field highly researched on to ensure the survival of a passenger in a car crash. This brings us to the crash detection and air bag deployment systems in the automotive industry. Frontal airbags drastically reduce harm to driver in frontal crashes by almost 30 percent and fatalities of front-seat passengers of age 13 and older by 32 percent (Survey from 2015). NHTSA estimates that as of 2015, a total of 44,869 lives have been saved primarily by frontal airbags (Survey 2017). At the instant of a crash, sensors start to measure severance of the impact. When the crash occurs beyond a set intensity, the sensors signal control unit to inflate the bags with gas within fractions of a second. The reference work analyzes a capacitive accelerometer capable of identifying positive and negative levels of acceleration along three perpendicular directions. However, this project is referred to a sensor capable of working with accelerations on an XY plane, on which it was built starting from a planar geometry. To understand this type of sensor the technological process with which modern semiconductor integrated circuits are manufactured is extensively used, thanks to which MEMS sensors are able to have dimensions in the order of nano meters. In case of a car accident, it is of utmost requirement that the airbag system reacts as fast as possible from the moment of the impact, in order to avoid fatal injuries. For this reason, it is necessary that the system analyses and give a response within the shortest possible time. The capacitive sensors are basically based on a moving solid body with a certain mass that will move when subjected to acceleration. The movement of the mass is the most important factor, because the small displacements of the structure leads (fingers and proof mass) to a variation of a capacity, as there are parts, called "fingers" that move closer or farther away depending on the direction of acceleration. These displacements are a direct effect of the acceleration on the system. When the capacity produced reaches a certain threshold value, it means that we are in a limit condition in the case under consideration; therefore, the system will react appropriately.

SYSTEM DETAILS

1) Proof mass: A proof mass or test mass is a known quantity of mass used in a measuring instrument as a reference for the measurement of an unknown quantity. A proof mass that deforms a spring in an accelerometer is sometimes called the seismic mass. This proof mass will have fingers attached to it on either side.

2) Spring: Thin beams placed in rectangular manner act as springs in the system. It facilitates movement to the proof mass, which in turn moves the fingers. The stiffness of these springs is the key parameter for displacement.

3) Fingers: Attached to the proof mass, these components are responsible to obtain differential capacitance. They are placed in between di-electric plates, such that a finger-gap and an anti- finger gap exists between them.

4) Connecting beams: these are used to connect the proof mass to the springs. 4 connecting beams are used with 2 for each spring.

5) Di-electric medium: Air is taken as the di-electric

(This work is licensed under a Creative Commons Attribution 4.0 International License.)

International Journal of Engineering Research & Technology (IJERT)
ISSN: 2278-0181
Vol. 10 Issue 08, August-2021

medium.

6) Anchors: A 100nm square cross section fixed joint, to which the springs are attached.

Density: 2320kg/m^3

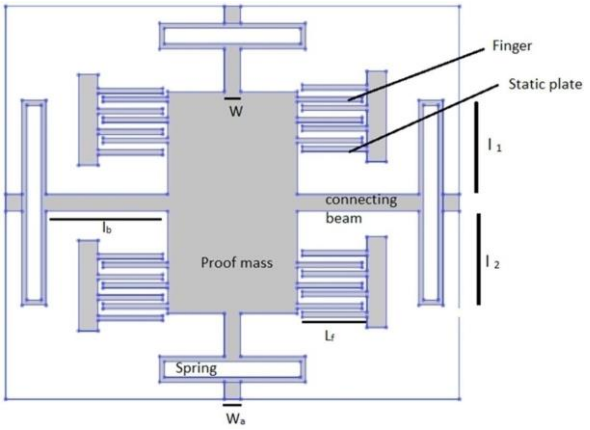

Fig .1.2.1 Parts of capacitive accelerometer Wa= Width of anchor

W= Width of connecting beam

lf= Length of fingers= Length of static plate l_1=l_2= Length of spring on either side

l_b= Length of connecting beam

Working of the System with Key Parameters

It is based on the movement of a proof mass to which are attached mobile fingers whose movement makes a change in capacity, that is calculated between them and the fixed fingers. From the displacement it can be traced back the acceleration value and the capacitive system is used to calculate it.

The instantaneous change in velocity (acceleration) on impact is converted into force on the system by Newtons laws of motion. This force is then responsible for the proof mass to move, which results in the movement of the fingers. A differential capacitance is set up at the gaps between the fingers and the di-electric plates. This capacitance produces a voltage which is transferred to the electronic control unit of the vehicle and if it is within the acceptable range causes the airbag t o deploy.

A force F, generated by external acceleration acting on the mass, m, causes a displacement x. The differential equation describing the system response is given by equation:

$$F(t)=m\partial^2x/\partial t^2+b\partial x/\partial t+Kx$$

b is the damping coefficient and K is the spring coefficient, the stiffness.

Displacement

F is both the force that will be induced to the mass of the system by the external acceleration, both the force given by Hooke's law that could be

7) Material of component: Polysilicon is chosen as the material of design with following properties:

The system can be depicted by a spring-mass-damper setup.

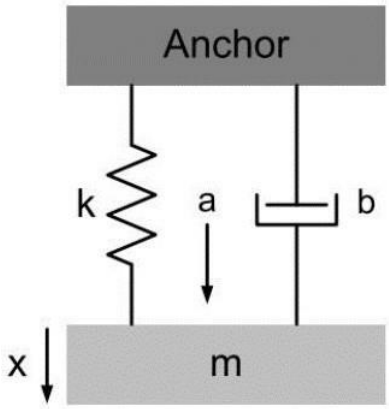

associated to the action of the springs, considering the stationary conditions. K is the spring's stiffness

Comparing the equations, displacement x can be given as:

x=ma/k…… (1)

This is the displacement obtained in x-direction for x-axis analysis

The same equation will hold good for y-direction:

Displacement y = ma/k…. (2)

(This work is licensed under a Creative Commons Attribution 4.0 International License.)

International Journal of Engineering Research & Technology (IJERT)
ISSN: 2278-0181
Vol. 10 Issue 08, August-2021

Capacitance

Capacitance of the system at a single finger between two dielectric plates(electrodes)n is given as

$$C=\epsilon_0 \times \epsilon_r \times A/d$$

ε0 is the dielectric permeability of the vacuum and is worth 8,854·10-12 F/m, ε_r is the dielectric permeability of the material that separates the armatures, in our case it is taken as 1F/m, considering that there will be only air, A is the total overlap surface between the electrodes and d is the gap from the finger. Finger gap-d1 and anti-finger gap d2 are taken in the ratio 1:2 respectively. This is done in order to discriminate the displacements in x and y axes. Thus, capacitance will be:

$$C=\epsilon_o\epsilon_r H L(1/d1+1/d2)$$

X-axis

When acceleration along the x-axis occurs, the capacity between the mobile and fixed fingers varies, because on the right the surface will increase by a factor x, the displacement, which will be added to the overlap length L and on the other side it will decrease, by the same amount.
So, for the two capacities their magnitude is given by:

$$C1=\epsilon_0\epsilon_r H\ (1/d_1+1/d_2)\ (L+x) \times F$$

$$C2=\epsilon_0\epsilon_r H\ (1/d_1+1/d_2)\ (L-x) \times F$$

Y-axis

When acceleration on the y-axis happens, the variation in capacity depends on the displacement that makes the distances d from the fingers vary. The change in capacity will depend on the displacement along the y-axis and further simplified substituting d1=2×d2

$C1=\epsilon_0\epsilon_r LH(1/(d_1-y)+1/(d_2+y)) \times F = \epsilon_0\epsilon_r LH\ (3d_1/(2d_1^2+d_1y-y^2)) \times F$

$C2=\epsilon_0\epsilon_r LH(1/(d_1+y)+1/(d_2-y)) \times F = \epsilon_0\epsilon_r LtH\ (3d_1/\ (2d_1^2-d_1y-y^2)) \times F$

A factor F of 6 is taken when 12 fingers are present in total, with 6 fingers contributing to C1 and equally forC2.
A factor F of 8 is taken when 16 fingers are present in total, with 8 fingers contributing to C1 and equally forC2.

Voltage:

The system is initially given a fixed amount of supply voltage, and once the differential capacitance is obtained, an output voltage signal will be sent to the control unit of the vehicle.

Vout = ((C1-C2)/ (C1+C2)) ×Vs

The following section of the report addresses some of the research work carried out by various researchers in the field of capacitive accelerometers and their extensive utilization for crash detection and airbag deployment. The research papers that were referred to are listed below:

Jesse Kendall, P.E. et.al [1] this paper gives an insight on the airbag deployment criteria and process

D S Dima et.al, 2017[2] this paper provides insight on the crash tests that can help the experts to identify the ranges of accelerations that may appear in various collision types. The correct sensors and data acquisition devices used in crash tests depend by the type of collisions.
Geeta Bhatt et.al, 2019[3] this paper provides insight on the importance of MEMS in the automotive industry along with the various applications in vehicles along with MEMS fabrication.
Vijayakumar S. et.al 2011 [4] this paper depicts the design and analysis of a 2-axis MEMS capacitive accelerometer
Divya et.aL, 2015[5] this paper provides insight on analysis of 3-axis accelerometers using COSMOL.
Gaurav Phulwari et.al, 2017[6] This paper provides insight on the importance of MEMS in the automotive industry and how they are cost effective, compact in size and help prevent major catastrophe.
Mourad Benmessaoud, 2013 [7] Optimization with respect to design parameters are done and variation are studied
Giulio Puccioni, 2020 [8] this paper provides insight on the performance of a standard capacitor accelerometer at varying accelerations and also provides insight on the effect of variation of thickness of the capacitive accelerometer.
Zakriya Mohammed 2016 [9] this paper optimizes finger spacing and spring constant and simulation is carried out.

Research Gap

The literature of displacement and stress analysis with respect to 2-axis MEMS capacitor accelerometer is scarce and doesn't involve alterations to the accelerometer to improve efficiency. The objective of our project is to design a 2-axis MEMS accelerometer and analyze the displacement and stress along the x and y axis. Certain alterations with respect to the design of the accelerometer are done to study the difference in performance.

1) **Objectives** To determine the total displacement with respect to acceleration variation(0-100g)

2) To determine the stress on x and y-axis

(This work is licensed under a Creative Commons Attribution 4.0 International License.)

International Journal of Engineering Research & Technology (IJERT)
ISSN: 2278-0181
Vol. 10 Issue 08, August-2021

Theoretical Analysis

- $W = V_{PM} \div L \times H$
- $M_{12F} = 12 \times M_{1F}$
- $M_{2LB} = 2 \times M_{LB}$
- $M_{2SB} = 2 \times M_{SB} = 4.64 \times 10^{-18}$ Kg
- $M_{tot} = M_{PM} + M_{12F} + V_{2LB} + M_{2SB}$
- Spring Stiffness $K = (\pi^4 \times E \times W \times H^3) / (6 \times (2L1)^3 + (2L2)^3)$
- $C1 = \epsilon 0 \epsilon r H (1/d1 + 1/d2) (L + x) \times 6$
- $C2 = \epsilon 0 \epsilon r H (1/d1 + 1/d2) (L - x) \times 6$
- 1. $C1 = \epsilon 0 \epsilon r L H (3d1/(2d1^2 + d1y - y^2)) \times 6$
- 2. $C2 = \epsilon_0 \epsilon_r L H (3d1/(2d1^2 - d1y - y^2)) \times 6$

Table 4.1.1 Result for acceleration in x-direction for the standard design

Acceleration m/s^2	Displacement x (fm)	C1($*10^{-17}$ F)	C2($*10^{-17}$ F)
0g	0	5.8941	5.8941
10g	3.4	5.8941	5.89405
20g	6.89	5.8941	5.89405
30g	10.33	5.8941	5.89405
40g	13.77	5.8941	5.89405
50g	17.22	5.8941	5.89405
60g	20.66	5.8941	5.89405
70g	24.11	5.8941	5.89405
80g	27.55	5.8941	5.89405
90g	31	5.8941	5.89405
100g	34.44	5.8941	5.89405

Displacement in y axis:

Displacement (y-direction) $y = (M \times 10g)/Ky = (1.129 \times 10^{-16} \times 10 \times 10)/9.74 = 1.15$ fm

Capacitance produced in y axis:

y-direction for the standard design

Acceleration m/s^2	Displacement y (fm)	C1($\times 10^{-17}$ F)	C2($\times 10^{-17}$ F)
0g	0	5.896764	5.896764
10g	1.32	5.896763806	5.896764194
20g	2.64	5.896763611	5.896764389
30g	3.96	5.896763413	5.896764584
40g	5.29	5.89676322	5.89676478
50g	6.61	5.896763026	5.896764974
60g	7.93	5.896762831	5.896765169
70g	9.25	5.896762636	5.896765364
80g	10.58	5.896762441	5.896765559
90g	11.9	5.896762246	5.896765754
100g	13.22	5.896762051	5.896765949

(This work is licensed under a Creative Commons Attribution 4.0 International License.)

International Journal of Engineering Research & Technology (IJERT)
ISSN: 2278-0181
Vol. 10 Issue 08, August-2021

Table 4.3.1 Result for acceleration in x-direction for thickness (20nm)

Acceleration m/s^2	Displacement x (fm)	C1(×10^{-17} F)	C2(×10^{-17} F)
0g	0	2.9483820	2.9483820
10g	24.02	2.9483822	2.948381808
20g	48.225	2.9483824	2.948381616
30g	72.34	2.9483826	2.948381424
40g	96.50	2.9483828	2.948381231
50g	120.50	2.9483830	2.948381040
60g	144.50	2.94838315	2.94838085
70g	168.8	2.94838335	2.948380655
80g	192.9	2.94838354	2.948380463
90g	217	2.94838373	2.948380271
100g	241.135	2.94838392	2.948380078

Table 4.3.2 Result for acceleration in y-direction for thickness(20nm)

Acceleration m/s^2	Displacement y (fm)	C1(×10^{-17} F)	C2(×10^{-17} F)
0g	0	2.9487	2.9487
10g	9.285	2.948698229	2.948700684
20g	18.57	2.948696445	2.948701369
30g	27.85	2.948694667	2.948702053
40g	37.135	2.948692886	2.948702738
50g	46.42	2.948691117	2.948703422
60g	55.705	2.94868935	2.948704106
70g	65	2.94868756	2.948704792
80g	74.25	2.94868578	2.948705474
90g	83.65	2.94868401	2.948706167
100g	92.845	2.94868223	2.948706844

Table 4.3.3 Result for acceleration in x-direction for thickness (80nm)

Acceleration m/s^2	Displacement x (fm)	C1(×10^{-17} F)	C2(×10^{-17} F)
0g	0	11.793528	11.793528
10g	0.5363	11.79352802	11.79352798
20g	1.073	11.79352803	11.79352797
30g	1.61	11.79352805	11.79352795
40g	2.145	11.79352802	11.79352793
50g	2.68	11.79352807	11.79352791
60g	3.22	11.79352810	11.79352790
70g	3.75	11.79352812	11.79352788
80g	4.29	11.79352814	11.79352786
90g	4.82	11.79352815	11.79352785
100g	5.36	11.79352817	11.79352783

Table 4.3.4 Result for acceleration in y-direction for thickness (80nm)

Acceleration m/s^2	Displacement y (fm)	C1(*10^{-17} F)	C2(*10^{-17} F)
0g	0	11.793528	11.793528
10g	0.144	11.79352796	11.79352804
20g	0.289	11.79352792	11.79352808
30g	0.435	11.79352787	11.79352813
40g	0.579	11.79352783	11.79352817
50g	0.724	11.7935278	11.79352822
60g	0.869	11.79352774	11.79352826
70g	1.014	11.7935277	11.79352830
80g	1.159	11.79352766	11.79352834
90g	1.30	11.79352762	11.79352838
100g	1.448	11.79352757	11.79352843

(This work is licensed under a Creative Commons Attribution 4.0 International License.)

International Journal of Engineering Research & Technology (IJERT)
ISSN: 2278-0181
Vol. 10 Issue 08, August-2021

Table 4.3.5 Result for acceleration in x-direction for thickness(160nm)

Acceleration m/s^2	Displacement x (fm)	C1(×10^{-17} F)	C2(×10^{-17} F)
0g	0	23.587056	23.587056
10g	0.0936	23.58705601	23.58705599
20g	0.187	23.58705601	23.58705599
30g	0.281	23.58705602	23.58705598
40g	0.375	23.58705602	23.58705598
50g	0.47	23.58705603	23.58705597
60g	0.562	23.58705604	23.58705596
70g	0.656	23.58705604	23.58705596
80g	0.75	23.58705605	23.58705595
90g	0.843	23.58705605	23.58705595
100g	0.937	23.58705606	23.58705594

Table 4.3.6 Result for acceleration in y-direction for thickness (160nm)

Acceleration m/s^2	Displacement y (fm)	C1(×10^{-17} F)	C2(×10^{-17} F)
0g	0	23.5875	23.5875
10g	0.036	23.58749998	23.58750002
20g	0.072	23.58749996	23.58750004
30g	0.108	23.58749994	23.58750006
40g	0.144	23.58749992	23.58750008
50g	0.180	23.58749989	23.58750011
60g	0.216	23.58749987	23.58750013
70g	0.252	23.58749985	23.58750015
80g	0.288	23.58749983	23.58750017
90g	0.324	23.58749981	23.58750019
100g	0.360	23.58749979	23.58750021

4.4 Additional Fingers and Reduction of Di-electric Gap

-

Table 4.4.1 Displacement for acceleration in x-direction for additional finger and reduced gap

Acceleration (m/s^2)	Displacement (fm)
0g	0
10g	3.5637
20g	7.1274
30g	10.691
40g	14.254
50g	17.818
60g	21.382
70g	24.946
80g	28.509
90g	32.0736
100g	35.637

Table4.4.2 Displacement for acceleration in y-direction for additional finger and reduced gap

Acceleration(m/s^2)	Displacement (fm)
0g	0
10g	1.368
20g	2.736
30g	4.105
40g	5.473
50g	6.842
60g	8.210
70g	9.578
80g	10.94
90g	12.31
100g	13.68

(This work is licensed under a Creative Commons Attribution 4.0 International License.)

International Journal of Engineering Research & Technology (IJERT)
ISSN: 2278-0181
Vol. 10 Issue 08, August-2021

Table 4.4.3 Capacitance for acceleration in x-direction for additional finger and reduced gap

Acceleration (m/s^2)	C1 ($\times 10^{-18}$ F)	C2($\times 10^{-18}$ F)
0	1.5724704	1.5724704
10	1.572470415	1.572470438
20	1.572470430	1.572470437
30	1.572470445	1.572470435
40	1.572470461	1.572470434
50	1.572470476	1.572470432
60	1.572470491	1.572470431
70	1.572470506	1.572470429
80	1.572470521	1.572470428
90	1.572470536	1.572470426
100	1.572470551	1.572470425

Table 4.4.4 Capacitance for acceleration in y-direction for additional finger and reduced gap

Acceleration (m/s^2)	C1 ($\times 10^{-18}$ F)	C2($\times 10^{-18}$ F)
0	1.5724704	1.5724704
10	1.5724702	1.5724705
20	1.5724701	1.5724706
30	1.5724700	1.5724707
40	1.5724699	1.5724708
50	1.5724698	1.5724709
60	1.5724697	1.5724710
70	1.5724696	1.5724711
80	1.5724695	1.5724712
90	1.5724694	1.5724713
100	1.5724693	1.5724714

CHAPTER **5**

5.1 Design

[All designs are done with a scale of 1nm=1mm]

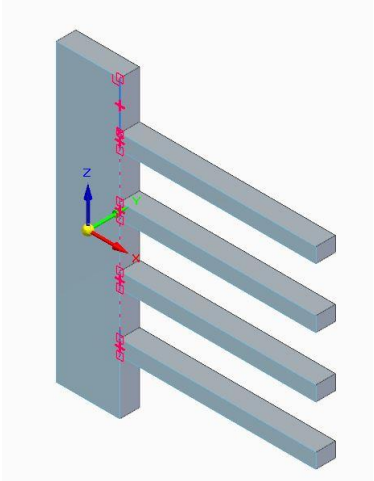

5.1.1 3D model of fixed finger

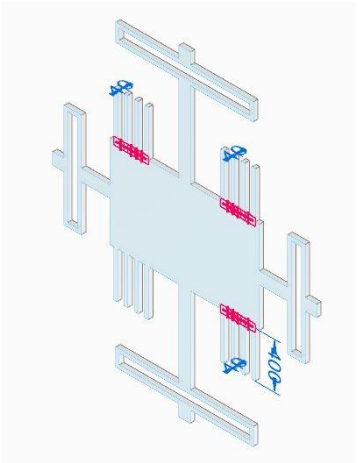

5.1.2 3D model of proof mass

(This work is licensed under a Creative Commons Attribution 4.0 International License.)

International Journal of Engineering Research & Technology (IJERT)
ISSN: 2278-0181
Vol. 10 Issue 08, August-2021

5.2 Design Of Standard Capacitance Accelerometer

The preliminary design was carried out on Solid edge . The design parameters of the standard capacitive accelerometer is taken from one of the research papers that were referred to. The fixed fingers and the proof mass along with fingers and springs were separately designed . The standard design has a total of 12 fingers on the proof mass. The thickness of both the proof mass and the fixed fingers are considered to be 40mm.

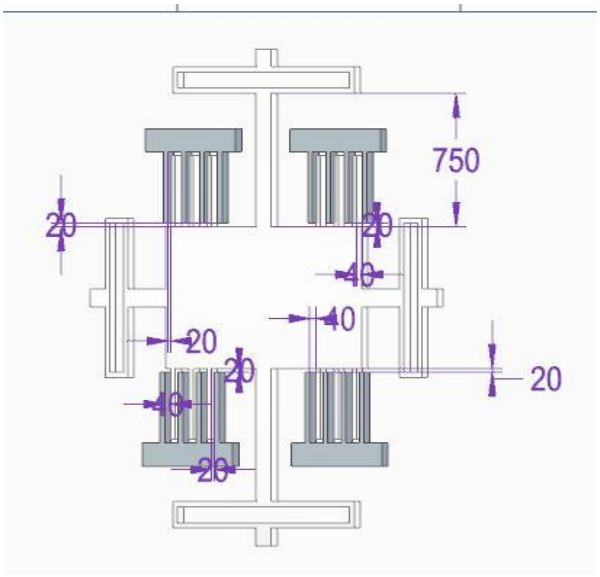

5.2.1 Standard capacitive accelerometer

5.3 Design Of Capacitance Accelerometer With Reduced Thickness Of 20mm

The thickness of both the proof mass and the fixed fingers are reduced by 20mm with respect to the standard design. There is no variation in any other parameters other than the thickness. The total number of fingers present in this model is 12. The proof mass and the fixed fingers are separately designed and assembled.

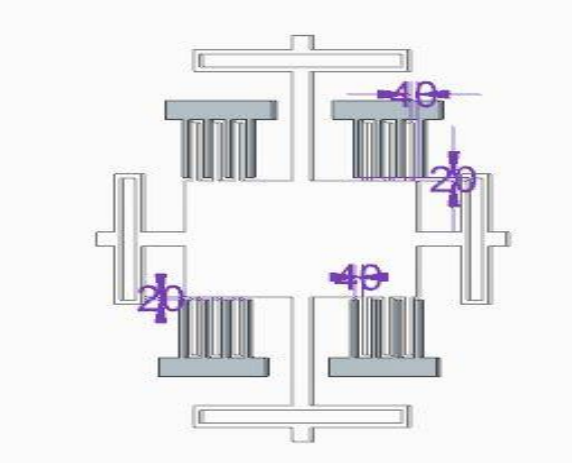

5.3.1 Capacitive accelerometer of thickness 20mm

(This work is licensed under a Creative Commons Attribution 4.0 International License.)

International Journal of Engineering Research & Technology (IJERT)
ISSN: 2278-0181
Vol. 10 Issue 08, August-2021

5.4 Design Of Capacitance Accelerometer With Increased Thickness Of 80mm

The thickness of both the proof mass and the fixed fingers are increased by 40mm with respect to the standard design. There is no variation in any other parameters other than the thickness. The total number of fingers present in this model is 12. The proof mass and the fixed fingers are separately designed and assembled.

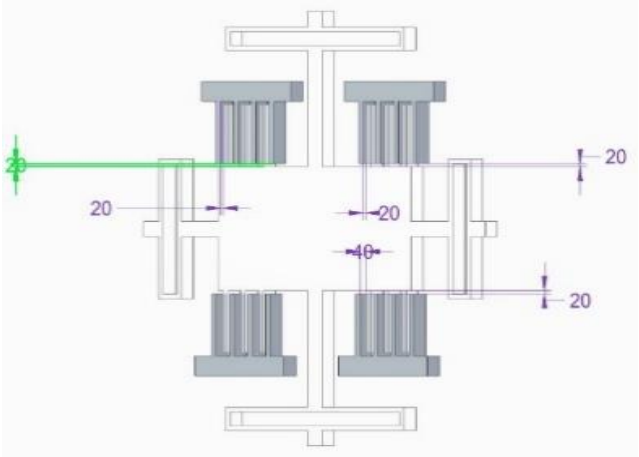

5.4.1 Capacitive accelerometer of thickness 80mm

5.5 Design Of Capacitance Accelerometer With Increased Thickness Of 160mm

The thickness of both the proof mass and the fixed fingers are increased by 120mm with respect to the standard design. There is no variation in any other parameters other than the thickness. The total number of fingers present in this model is 12. The proof mass and the fixed fingers are separately designed and assembled.

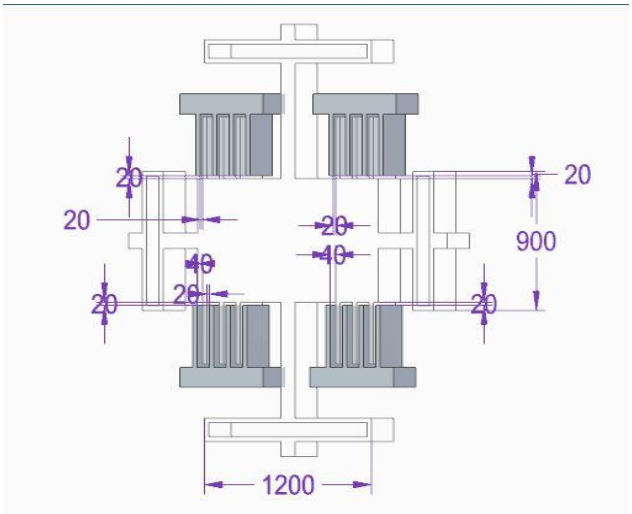

5.5.1 Capacitive accelerometer of thickness 160mm

(This work is licensed under a Creative Commons Attribution 4.0 International License.)

International Journal of Engineering Research & Technology (IJERT)
ISSN: 2278-0181
Vol. 10 Issue 08, August-2021

5.6 Design Of Capacitance Accelerometer With Additional Fingers with same c/s

The fixed fingers and the proof mass along with fingers and springs were separately designed . The standard design has a total of 16 fingers on the proof mass. The thickness of both the proof mass and the fixed fingers are considered to be 40mm. The proof mass and the fixed fingers are separately designed and assembled.

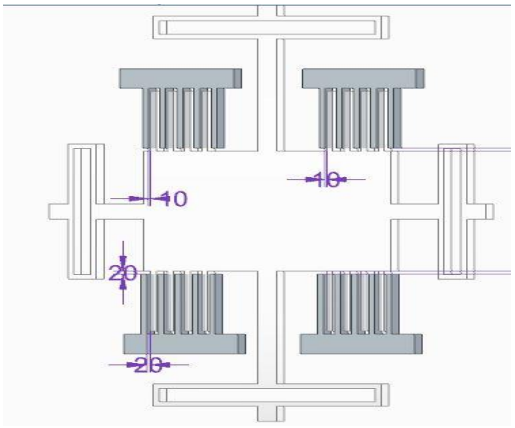

5.6.1 Capacitive accelerometer with additional fingers

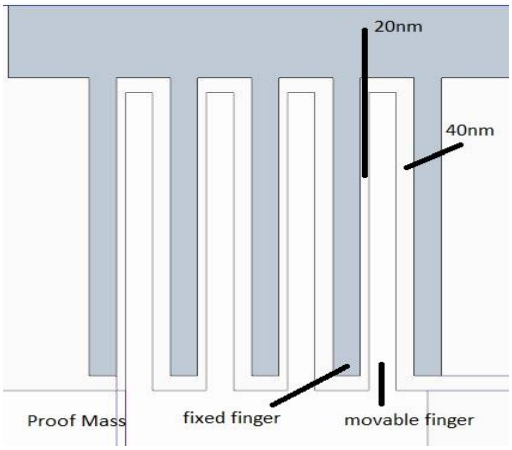

5.6.2 Gap between fingers

CHAPTER 6

Analysis

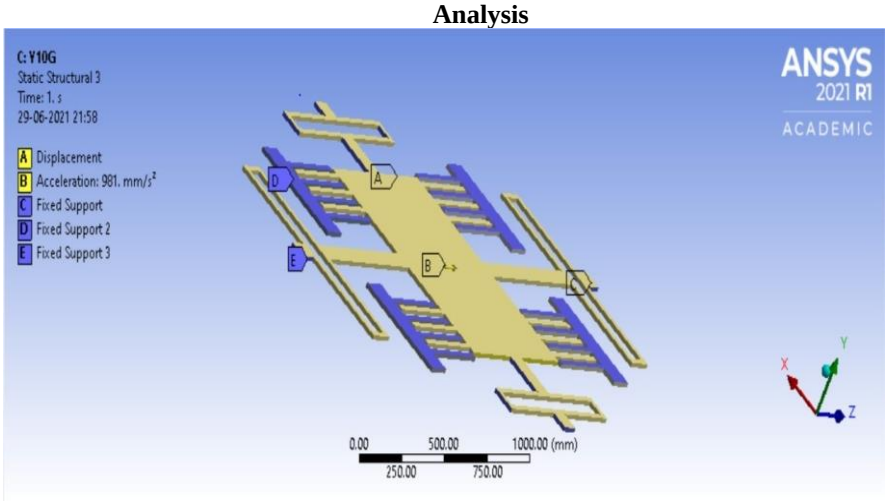

Fig 6.1: Load and constraints under structural analysis

The model is scaled as per 1nm=1mm in the simulation process.

6.1 Standard model:

The stress analysis is done on the software called ANSYS. First the assembly created on solid edge is converted to a .igs file which makes it compatible with ANSYS. The assembly is then transferred to ANSYS via the DesignModeler.

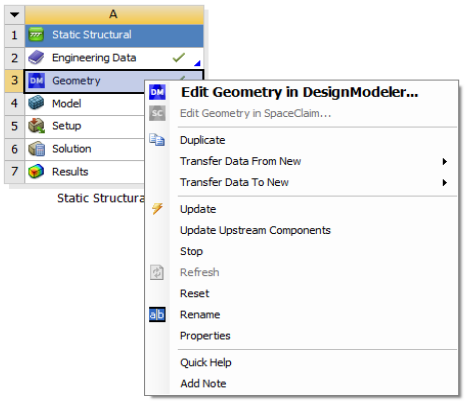

(This work is licensed under a Creative Commons Attribution 4.0 International License.)

International Journal of Engineering Research & Technology (IJERT)
ISSN: 2278-0181
Vol. 10 Issue 08, August-2021

After importing the assembly the in the DesignModeler, a face split is performed to separate the proof mass from the fingers and the connecting rods.

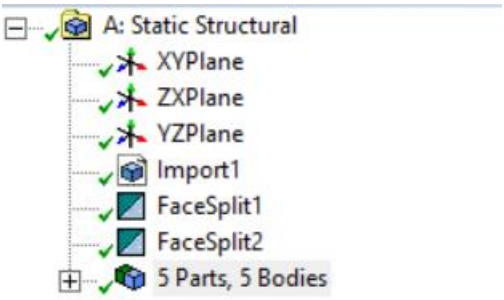

The material is selected to be silicon anisotropic for the analysis. The design is then meshed with a size of 50mm.

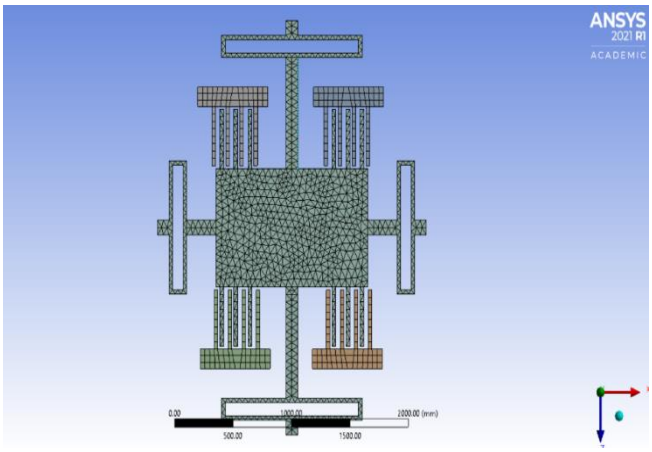

Fig 6.2: Meshed model in Ansys

The acceleration is set to the proof mass for 10G in the x axis , and a displacement of 0mm is set in the x axis. The Fixed fingers are considered as fixed constraints. The larger springs are also constrained as the analysis is strictly performed for the x axis.

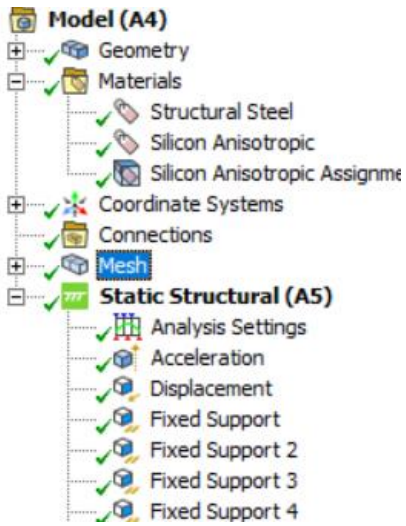

(This work is licensed under a Creative Commons Attribution 4.0 International License.)

International Journal of Engineering Research & Technology (IJERT)
ISSN: 2278-0181
Vol. 10 Issue 08, August-2021

The total deformation analysis is performed and results are obtained for 10G , 30G ,50G ,70G and 100G respectively.

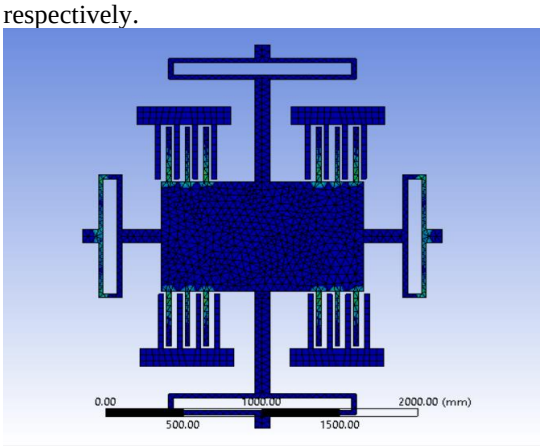

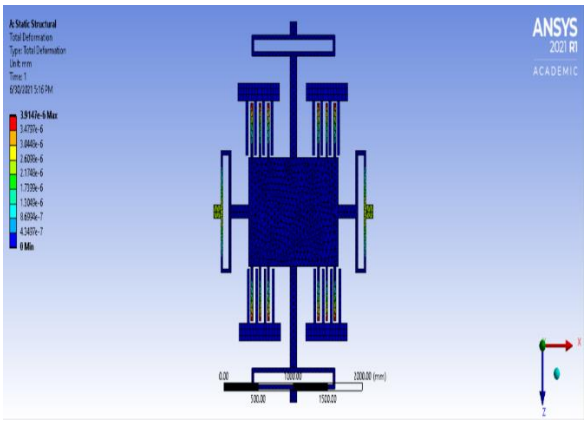

Fig: 6.3 Stress distribution for standard model x-axis simulation AND
Fig 6.4: Displacement under x-axis simulation for standard model

Similarly the same procedure is followed for analysis of stress in the y axis. Instead of constraining the larger springs , the smaller springs are constrained. The acceleration is considered to be 10G and the displacement is considered to be 0mm in z axis. The total deformation is analyzed for 10G , 30G , 50G . 70G and 100G respectively.

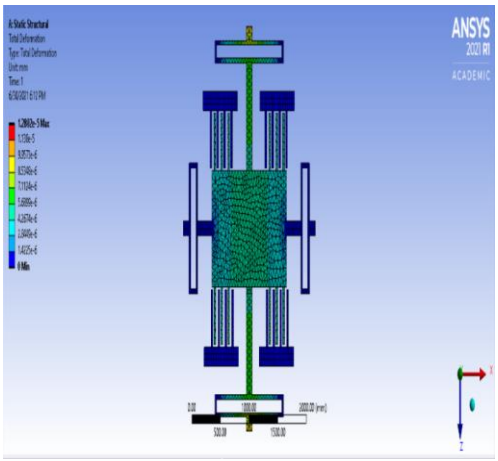

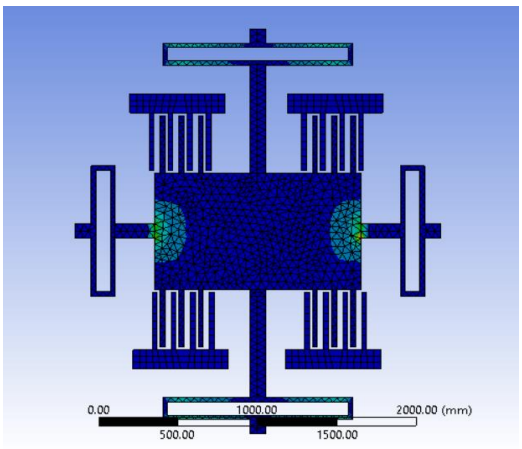

Fig 6.5: Displacement in yaxis for standard model AND Fig6.6 : Stress displacements in y axis for standard model.

6.2 Model with thickness of 20mm: .

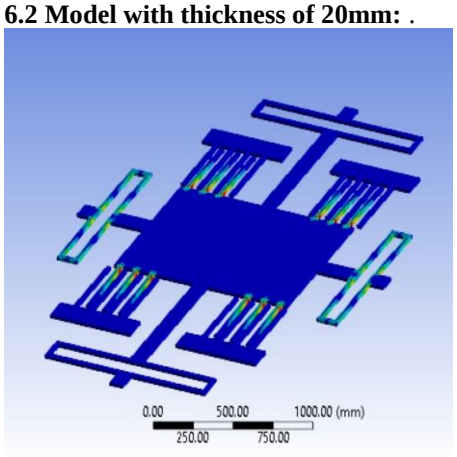

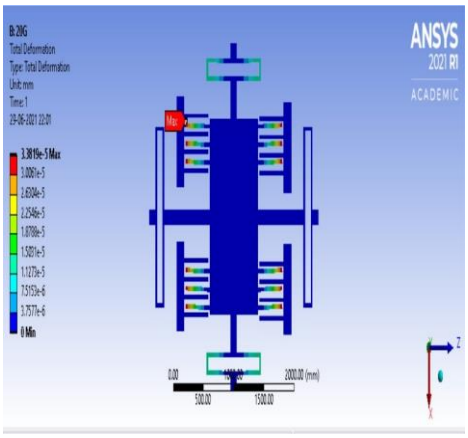

Fig 6.2.1 stress for x-axis simulation Fig 6.2.2Displacement for x-axis simulation

(This work is licensed under a Creative Commons Attribution 4.0 International License.)

International Journal of Engineering Research & Technology (IJERT)
ISSN: 2278-0181
Vol. 10 Issue 08, August-2021

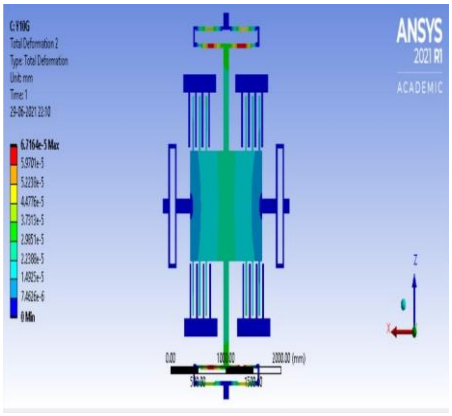

Fig 6.2.3 Displacement for y-axis simulation

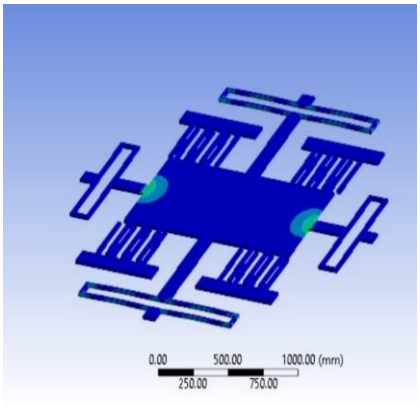

Fig 6.2.4 Stress distribution for y-axis simulation

6.3 Model with thickness of 80mm

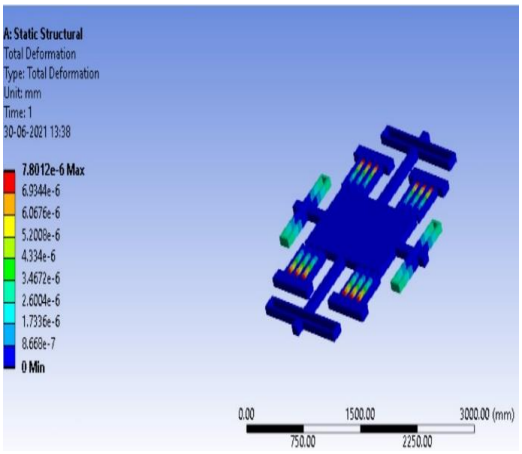

Fig 6.3.1Displacement for x-axis simulation

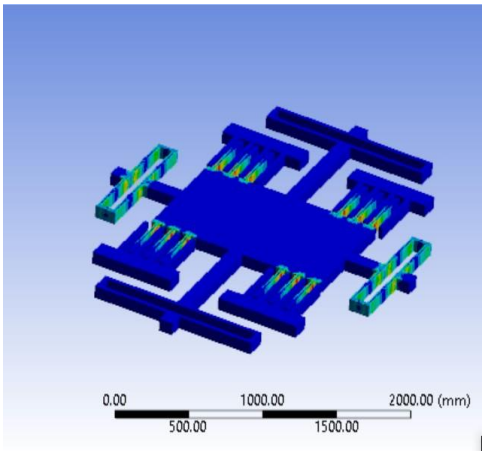

Fig 6.3.2 Stress distribution x-axis simulation

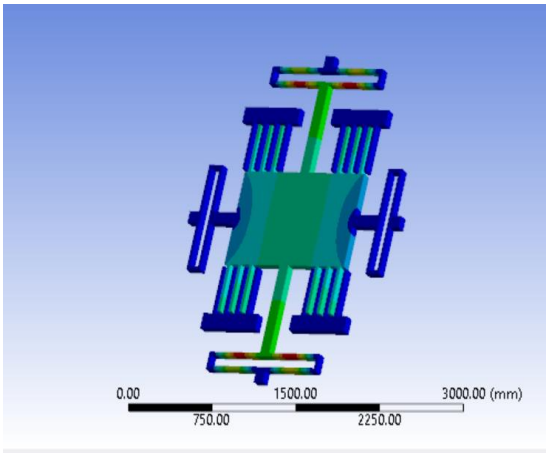

Fig 6.3.3 Displacement for y-axis simulation

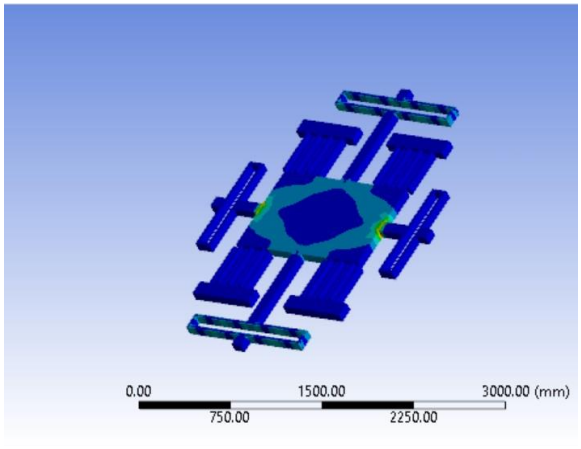

Fig 6.3.4 Stress distribution for y-axis simulation

(This work is licensed under a Creative Commons Attribution 4.0 International License.)

International Journal of Engineering Research & Technology (IJERT)
ISSN: 2278-0181
Vol. 10 Issue 08, August-2021

6.4 Model with thickness of 160mm:

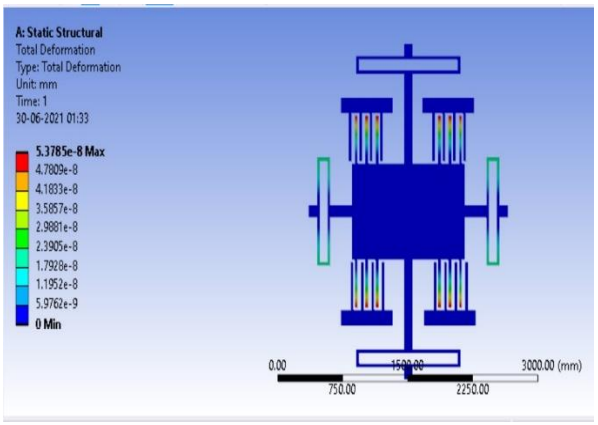

Fig 6.4.1 Displacement for x-axis simulation

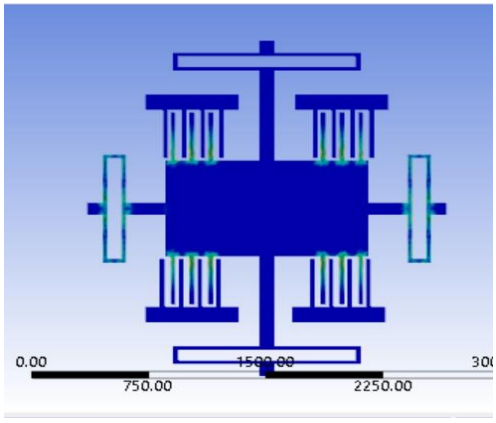

Fig 6.4.2Stress distribution for x-axis simulation

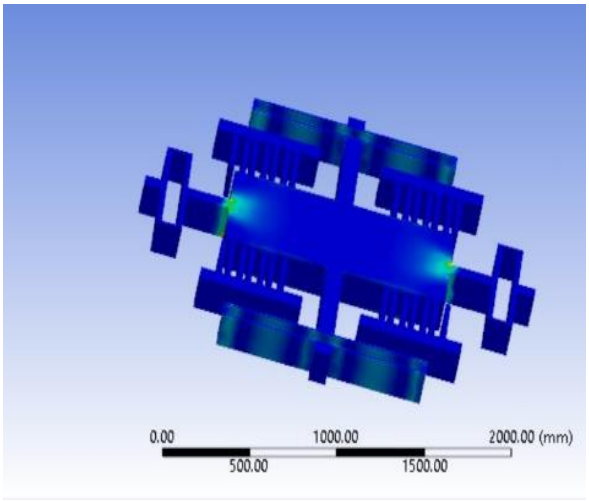

Fig 6.4.4 Stress distribution for y-axis simulation

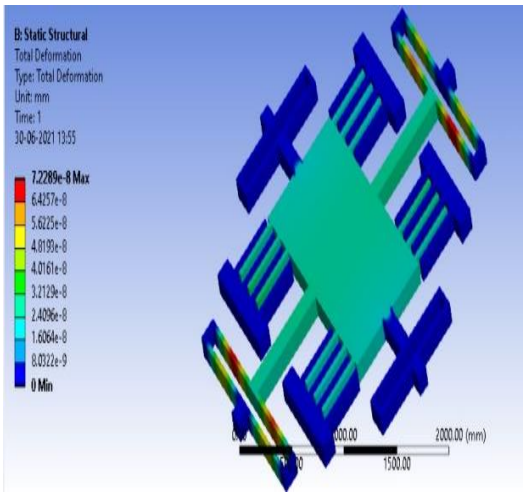

Fig6.4.3 Displacement for y-axis simulation

6.5 Model with Additional Fingers:

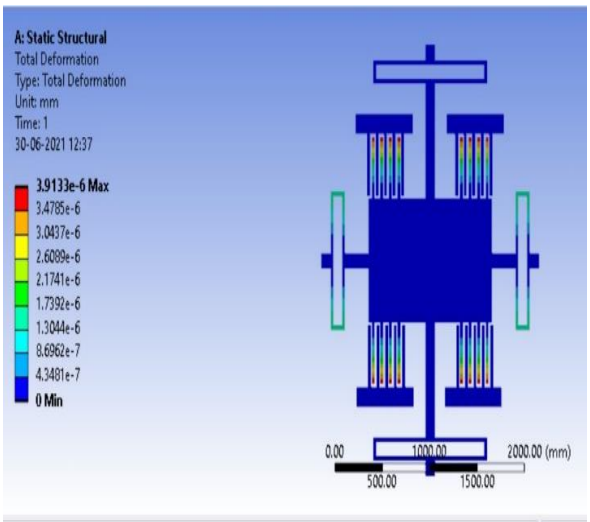

Fig 6.5.1Displacement for x-axis simulation

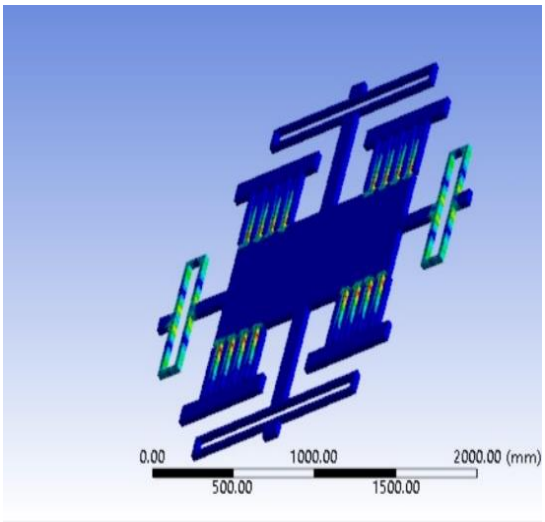

Fig 6.5.2 Stress distribution for x-axis simulation

(This work is licensed under a Creative Commons Attribution 4.0 International License.)

International Journal of Engineering Research & Technology (IJERT)
ISSN: 2278-0181
Vol. 10 Issue 08, August-2021

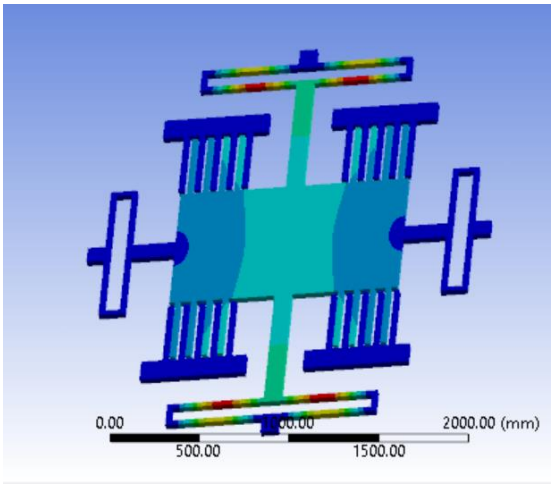

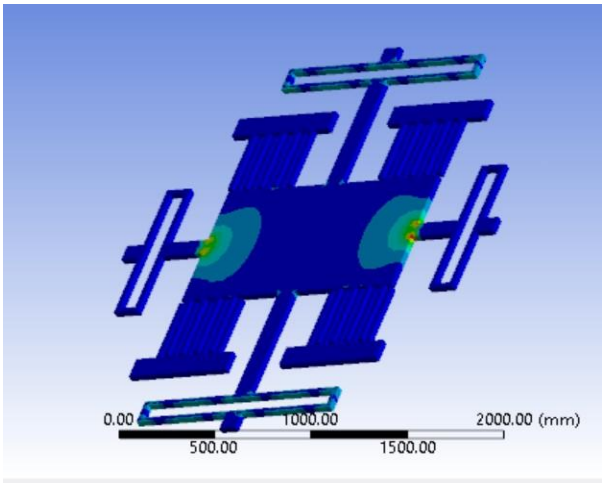

Fig 6.5.3 Displacement for y-axis simulation Fig 6.5.4 Stress distribution for y-axis simulation

6.7 Results:

6.7.1 Result for acceleration in x-direction for the standard design

Acceleration m/s^2	Displacement x (fm)
10g	3.91
30g	11.74
50g	19.57
70g	27.40
100g	39.147

6.7.2 Result for acceleration in y-direction for the standard design

Acceleration m/s^2	Displacement y (fm)
10g	0.12
30g	1.2802
50g	3.8407
70g	6.4011
100g	8.9616

6.7.3 Result for acceleration in x-direction for thickness (20nm)

Acceleration m/s^2	Displacement y (fm)
10g	33.8
30g	99.6
50g	167
70g	236
100g	338

6.7.4 Result for acceleration in y-direction for thickness (20nm)

Acceleration m/s^2	Displacement y (fm)
10g	6.7
30g	19.7
50g	33.5
70g	47
100g	68

(This work is licensed under a Creative Commons Attribution 4.0 International License.)

International Journal of Engineering Research & Technology (IJERT)
ISSN: 2278-0181
Vol. 10 Issue 08, August-2021

6.7.5 Result for acceleration in x-direction for thickness (80nm)

Acceleration m/s^2	Displacement y (fm)
10g	0.78
30g	2.34
50g	3.6
70g	5.4
100g	9.78

6.7.6 Result for acceleration in y-direction for thickness (80nm)

Acceleration m/s^2	Displacement y (fm)
10g	0.076
30g	0.23
50g	0.38
70g	0.52
100g	0.76

6.7.7 Result for acceleration in x-direction for thickness (160nm)

Acceleration m/s^2	Displacement y (fm)
10g	0.0768
30g	0.211
50g	0.384
70g	0.53
100g	0.768

6.7.8 Result for acceleration in y-direction for thickness (160nm)

Acceleration m/s^2	Displacement y (fm)
10g	0.076
30g	0.21
50g	0.34
70g	0.48
100g	0.69

6.7.9 Result for acceleration in x-direction for altered number of fingers

Acceleration m/s^2	Displacement y (fm)
10g	3.9
30g	11.74
50g	19.56
70g	27.4
100g	32.67

6.7.10 Result for acceleration in y-direction for altered number of fingers

Acceleration m/s^2	Displacement y (fm)
10g	0.69
30g	2.07
50g	3.45
70g	4.8
100g	6.9

(This work is licensed under a Creative Commons Attribution 4.0 International License.)

International Journal of Engineering Research & Technology (IJERT)
ISSN: 2278-0181
Vol. 10 Issue 08, August-2021

Conclusion

$$C = \varepsilon_0(\frac{A}{d})$$

Capacitance relation to displacement obtained:
The analysis conducted indicates that with increase in the thickness of the capacitive accelerometer, the displacement decreases which in turn increases the capacitance induced. With increase in capacitance induced the response time of the airbag control module is reduced, thus increasing the efficiency of accelerometer by increasing the thickness of the capacitive accelerometer also increases the stress induced in the accelerometer. So, we have to compromise with the efficiency of the accelerometer due to the stress produced. The basic standard of capacitive accelerometer available in market generally has a dimension of 40mm thickness.

Stress analysis:
Stress analysis was carried out to analyze critical points of failure under the action of loads. Thus, what can be inferred from this is that, for application of load in x direction, the maximum stress is concentrated at the point where the fingers are attached to the proof mass. For the y-axis analysis, the stress was observed to be concentrated at the point where the lateral connecting beams are attached to the proof mass.

Future Work

The entire work was carried out based on the fingers placed in the lateral position only (along x-axis) even for the y-axis simulations. Thus, one of the major improvements to the model can be the introduction of sensing fingers on the y-axis that is along the longitudinal direction as well. This will further enhance the system efficiency particularly for longitudinal analysis.
The work carried out can further be improved and a more idealistic and justified results can be obtained taking into consideration the COMSOL software approach. The model can be taken its true scale and boundary conditions will remain the same as in case of the work carried out above.

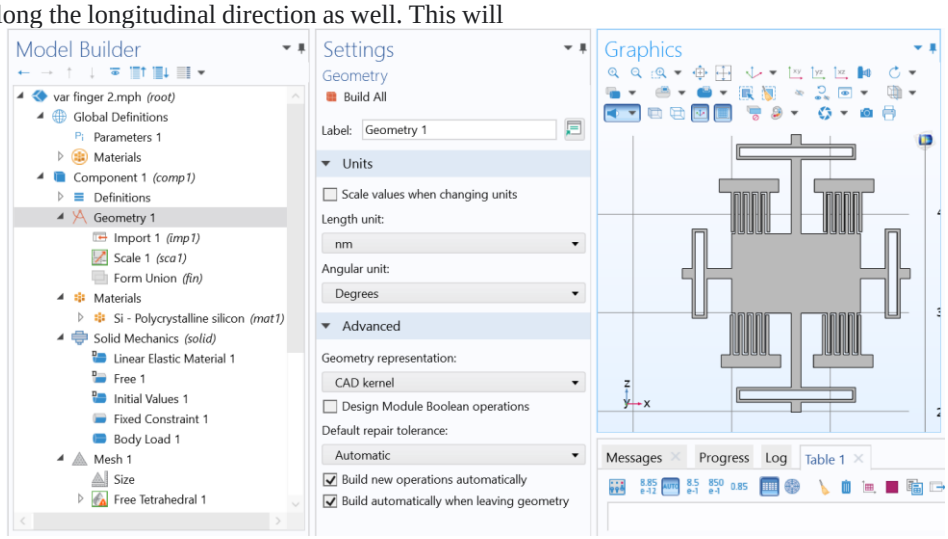

Fig 9.1: COMSOL approach – static structural

Two primary modules are taken into consideration. One is the solid mechanics module that deals with the static structural analysis of displacement and stress of the body.
The next is the Electro Statics Module which deals with determination of differential capacitance at the terminals required. A reference voltage of 1V is applied to the fixed terminals and the proof mass will be at ground charge condition. This is analyzed under electric potential probe analysis to determine output voltage and maxwell differential capacitances can be obtained in tabulated format.

(This work is licensed under a Creative Commons Attribution 4.0 International License.)

International Journal of Engineering Research & Technology (IJERT)
ISSN: 2278-0181
Vol. 10 Issue 08, August-2021

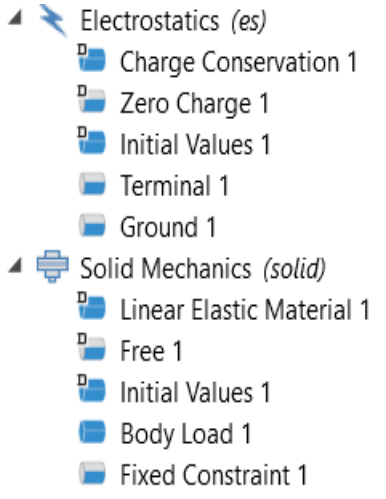

Fig 9.2: Modules and conditions

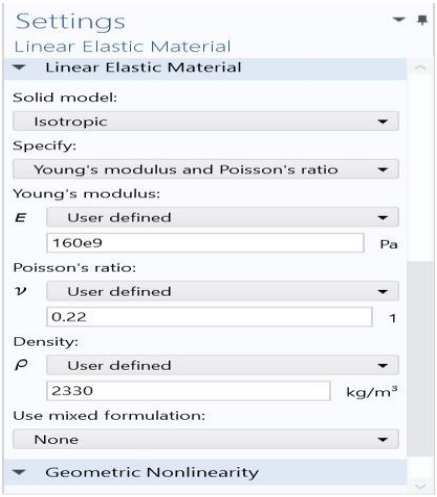

Fig9.3: System properties

In order to analyze the capacitance produced by the capacitive accelerometer an electrostatics study was conducted in COMSOL. The fixed fingers are given an terminal voltage value of 1V. The proof mass along with the moveable fingers are grounded. A body load is defined with respect to volume on the proof mass. The fixed constraints are applied on the fixed fingers. A global probe is created to determine the Maxwell capacitance.

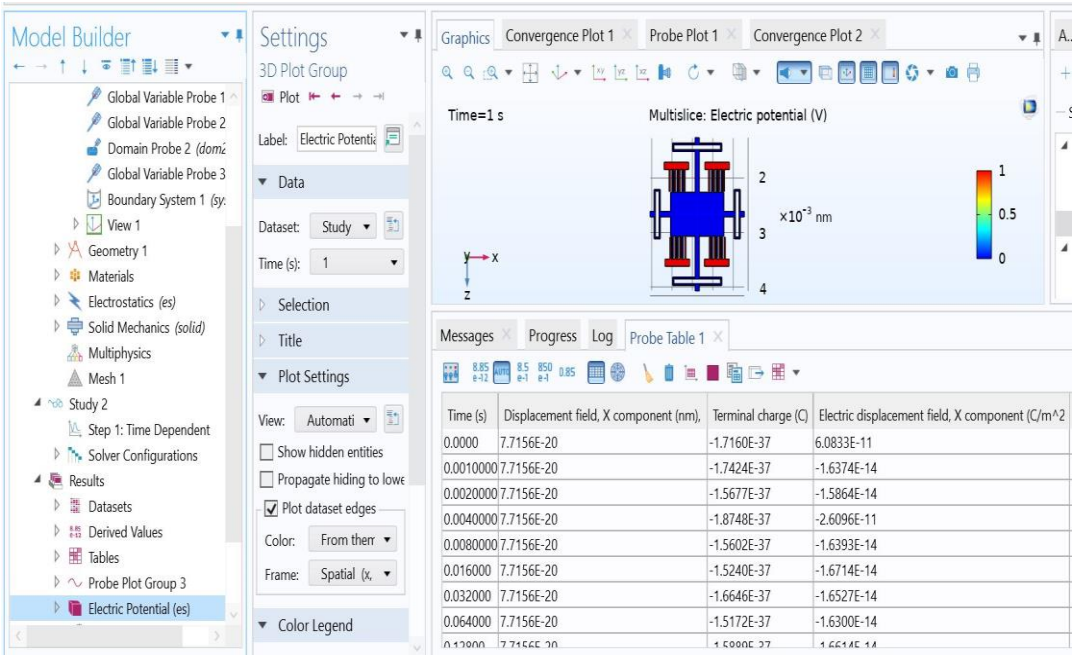

Fig9.4 : Electrostatic comsol approach

Thus, through this approach, both static structural and electrostatics can give conclusive evidence on the efficiency of the system, through both static analysis and electrical approach.

Dynamic Analysis

Another Approach to obtain precise outputs is the dynamic analysis of the system in time dependent form. Due to lack of system requirements and license of software being limited to use, this approach was not possible to be done. However, in future prospects, this will definitely enhance the results and give justified outputs for effective efficiency comparison between the models.

However, A transient structural (time variant) approach was carried out in subsets for a time interval of 1s starting from 0.2

(This work is licensed under a Creative Commons Attribution 4.0 International License.)

International Journal of Engineering Research & Technology (IJERT)
ISSN: 2278-0181
Vol. 10 Issue 08, August-2021

seconds in steps of 0.1 /0.15 seconds up to 16 subsets. It was observed that the deformation is more or less the same as in case of static structural, but a very small decrease in deformation was seen half way through the time interval and the certain small variations of increase-decrease took place, after which, the value increases and maximum value is obtained. Acceleration, displacement and fixed constraints would remain the same as in static structural analysis.

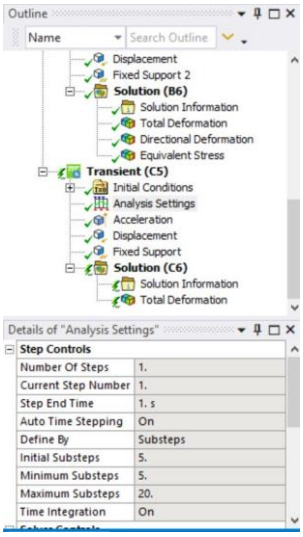

Fig9.5: Transient analysis setup

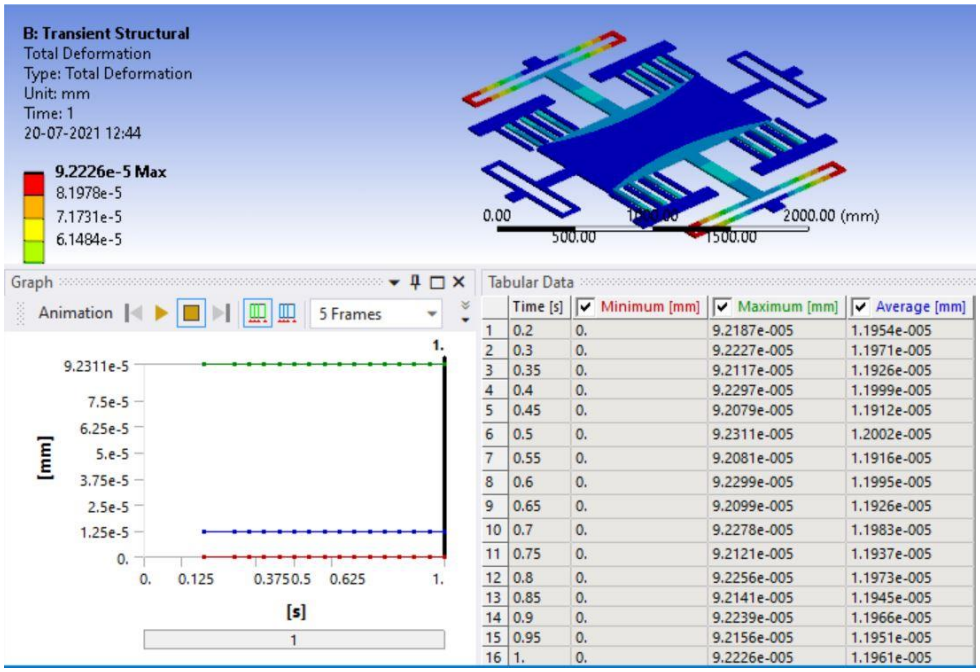

Fig 9.6: Transient analysis 20nm y axis

(This work is licensed under a Creative Commons Attribution 4.0 International License.)

International Journal of Engineering Research & Technology (IJERT)
ISSN: 2278-0181
Vol. 10 Issue 08, August-2021

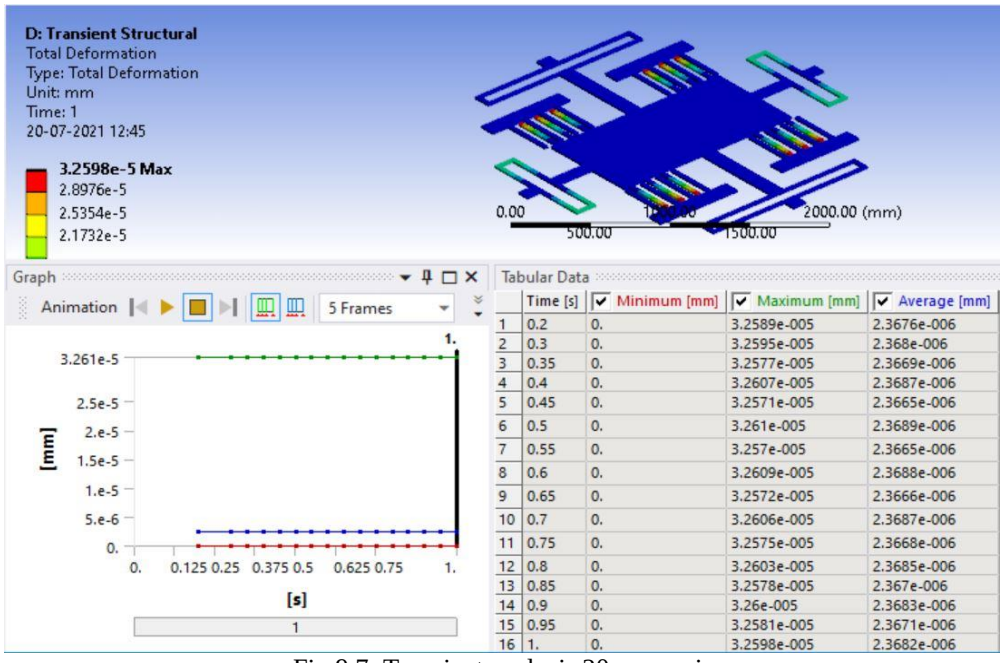

	Time [s]	Minimum [mm]	Maximum [mm]	Average [mm]
1	0.2	0.	3.2589e-005	2.3676e-006
2	0.3	0.	3.2595e-005	2.368e-006
3	0.35	0.	3.2577e-005	2.3669e-006
4	0.4	0.	3.2607e-005	2.3687e-006
5	0.45	0.	3.2571e-005	2.3665e-006
6	0.5	0.	3.261e-005	2.3689e-006
7	0.55	0.	3.257e-005	2.3665e-006
8	0.6	0.	3.2609e-005	2.3688e-006
9	0.65	0.	3.2572e-005	2.3666e-006
10	0.7	0.	3.2606e-005	2.3687e-006
11	0.75	0.	3.2575e-005	2.3668e-006
12	0.8	0.	3.2603e-005	2.3685e-006
13	0.85	0.	3.2578e-005	2.367e-006
14	0.9	0.	3.26e-005	2.3683e-006
15	0.95	0.	3.2581e-005	2.3671e-006
16	1.	0.	3.2598e-005	2.3682e-006

Fig 9.7: Transient analysis 20nm x axis

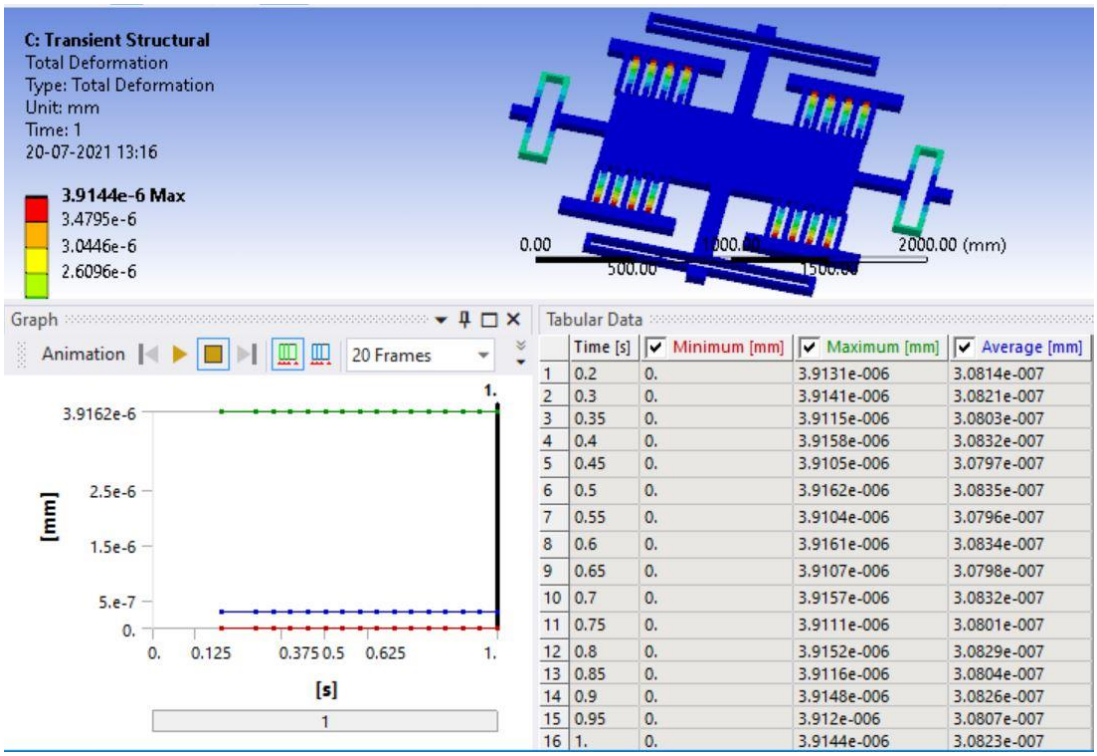

	Time [s]	Minimum [mm]	Maximum [mm]	Average [mm]
1	0.2	0.	3.9131e-006	3.0814e-007
2	0.3	0.	3.9141e-006	3.0821e-007
3	0.35	0.	3.9115e-006	3.0803e-007
4	0.4	0.	3.9158e-006	3.0832e-007
5	0.45	0.	3.9105e-006	3.0797e-007
6	0.5	0.	3.9162e-006	3.0835e-007
7	0.55	0.	3.9104e-006	3.0796e-007
8	0.6	0.	3.9161e-006	3.0834e-007
9	0.65	0.	3.9107e-006	3.0798e-007
10	0.7	0.	3.9157e-006	3.0832e-007
11	0.75	0.	3.9111e-006	3.0801e-007
12	0.8	0.	3.9152e-006	3.0829e-007
13	0.85	0.	3.9116e-006	3.0804e-007
14	0.9	0.	3.9148e-006	3.0826e-007
15	0.95	0.	3.912e-006	3.0807e-007
16	1.	0.	3.9144e-006	3.0823e-007

Fig 9.8: Varied finger x axis transient analysis

(This work is licensed under a Creative Commons Attribution 4.0 International License.)

International Journal of Engineering Research & Technology (IJERT)
ISSN: 2278-0181
Vol. 10 Issue 08, August-2021

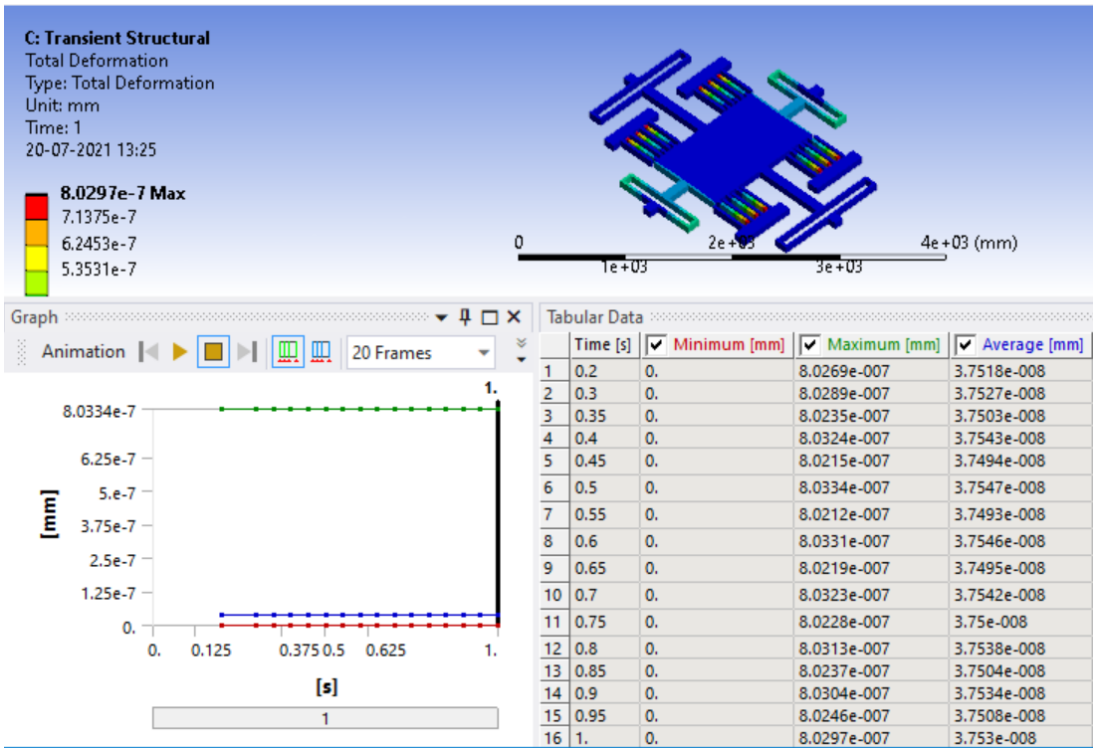

	Time [s]	Minimum [mm]	Maximum [mm]	Average [mm]
1	0.2	0.	8.0269e-007	3.7518e-008
2	0.3	0.	8.0289e-007	3.7527e-008
3	0.35	0.	8.0235e-007	3.7503e-008
4	0.4	0.	8.0324e-007	3.7543e-008
5	0.45	0.	8.0215e-007	3.7494e-008
6	0.5	0.	8.0334e-007	3.7547e-008
7	0.55	0.	8.0212e-007	3.7493e-008
8	0.6	0.	8.0331e-007	3.7546e-008
9	0.65	0.	8.0219e-007	3.7495e-008
10	0.7	0.	8.0323e-007	3.7542e-008
11	0.75	0.	8.0228e-007	3.75e-008
12	0.8	0.	8.0313e-007	3.7538e-008
13	0.85	0.	8.0237e-007	3.7504e-008
14	0.9	0.	8.0304e-007	3.7534e-008
15	0.95	0.	8.0246e-007	3.7508e-008
16	1.	0.	8.0297e-007	3.753e-008

Fig 9.9: 80nm model transient analysis (x-axis)

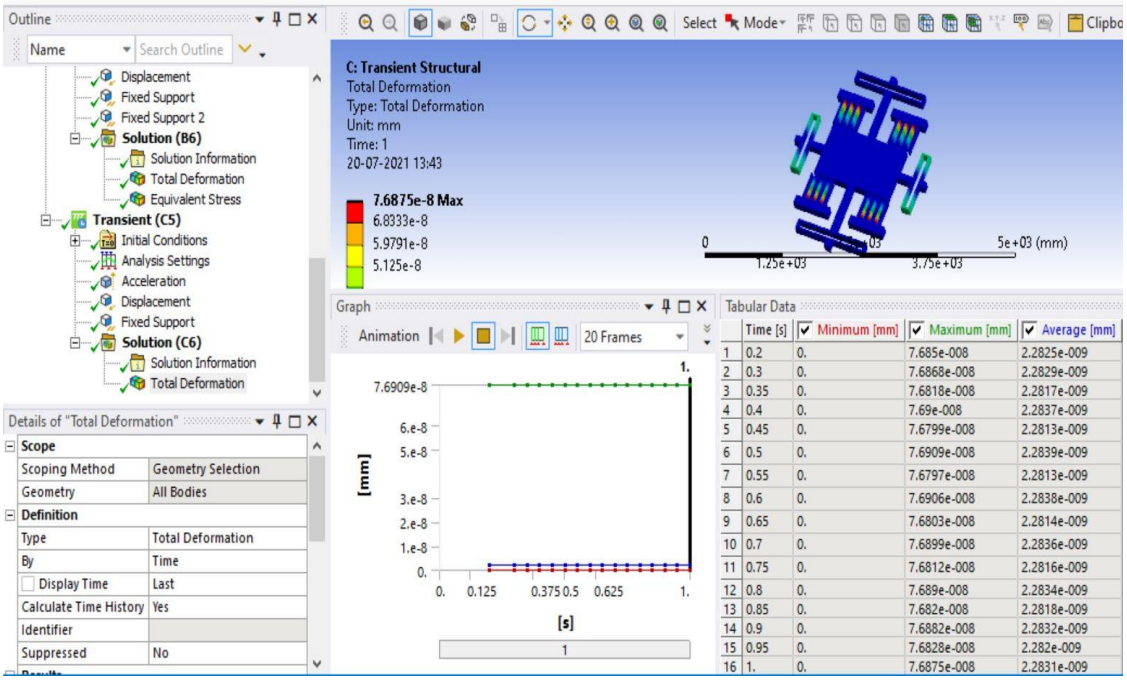

	Time [s]	Minimum [mm]	Maximum [mm]	Average [mm]
1	0.2	0.	7.685e-008	2.2825e-009
2	0.3	0.	7.6868e-008	2.2829e-009
3	0.35	0.	7.6818e-008	2.2817e-009
4	0.4	0.	7.69e-008	2.2837e-009
5	0.45	0.	7.6799e-008	2.2813e-009
6	0.5	0.	7.6909e-008	2.2839e-009
7	0.55	0.	7.6797e-008	2.2813e-009
8	0.6	0.	7.6906e-008	2.2838e-009
9	0.65	0.	7.6803e-008	2.2814e-009
10	0.7	0.	7.6899e-008	2.2836e-009
11	0.75	0.	7.6812e-008	2.2816e-009
12	0.8	0.	7.689e-008	2.2834e-009
13	0.85	0.	7.682e-008	2.2818e-009
14	0.9	0.	7.6882e-008	2.2832e-009
15	0.95	0.	7.6828e-008	2.282e-009
16	1.	0.	7.6875e-008	2.2831e-009

Fig 9.10: 160nm model transient analysis (x-axis)

(This work is licensed under a Creative Commons Attribution 4.0 International License.)

International Journal of Engineering Research & Technology (IJERT)
ISSN: 2278-0181
Vol. 10 Issue 08, August-2021

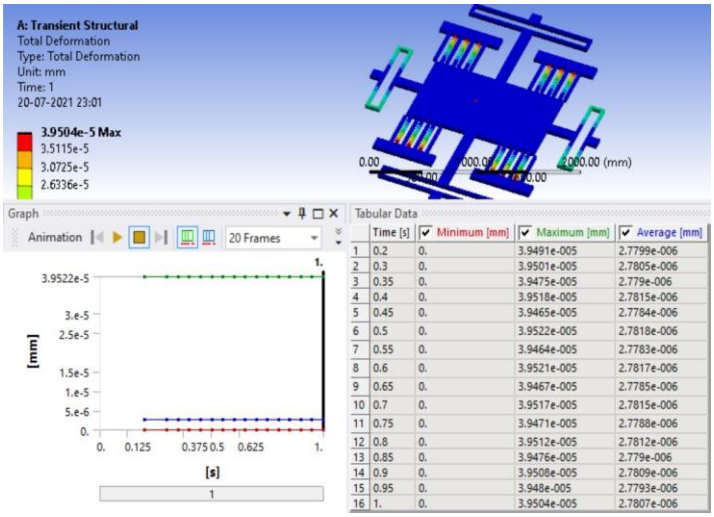

	Time [s]	Minimum [mm]	Maximum [mm]	Average [mm]
1	0.2	0.	3.9491e-005	2.7799e-006
2	0.3	0.	3.9501e-005	2.7805e-006
3	0.35	0.	3.9475e-005	2.779e-006
4	0.4	0.	3.9518e-005	2.7815e-006
5	0.45	0.	3.9465e-005	2.7784e-006
6	0.5	0.	3.9522e-005	2.7818e-006
7	0.55	0.	3.9464e-005	2.7783e-006
8	0.6	0.	3.9521e-005	2.7817e-006
9	0.65	0.	3.9467e-005	2.7785e-006
10	0.7	0.	3.9517e-005	2.7815e-006
11	0.75	0.	3.9471e-005	2.7788e-006
12	0.8	0.	3.9512e-005	2.7812e-006
13	0.85	0.	3.9476e-005	2.779e-006
14	0.9	0.	3.9508e-005	2.7809e-006
15	0.95	0.	3.948e-005	2.7793e-006
16	1.	0.	3.9504e-005	2.7807e-006

Fig 9.11 Standard model transient analysis

REFERENCES:

[1] Occupant Protection in Passenger Vehicles, Traffic Safety Facts 2017 Data https://crashstats.nhtsa.dot.gov/Api/Public/ViewPublication/812691

[2] Accelerometers: Taking the Guesswork out of Accelerometer Selection https://blog.endaq.com/accelerometer-selection

[3] Niu, W. , Fang, L. , Xu, L. , Li, X. , Huo, R. , Guo, D. and Qi, Z. (2018) Summary of Research Status and Application of MEMS Accelerometers. Journal of Computer and Communications, 6, 215-221. doi: 10.4236/jcc.2018.612021.

[4] Accelerometer Sensor Working and Applications https://www.elprocus.com/accelerometer-sensor-working-and-applications/

[5] Puccioni, Giulio. (11 February 2020). "Design and Analysis of MEMS Capacitive Accelormeter "

[6] G. Vijila, S. Vijayakumar, M. Alagappan, and A. Gupta(2011) " Design and Analysis of 3D Capacitive Accelerometer for Automotive Applications" https://www.comsol.co.in/paper/design-and-analysis-of-3d-capacitive-accelerometer-for-automotive-applications-1146

[7] Vinay, P & Satya, Ch & Vamsi, Sri & Hemanth, M & Saiteja, A & Ali, .abid & Puli, Ashok & Satya, Venkata. (2017). Design and simulation of MEMS based accelerometer for crash detection and air bags deployment in automobiles. International Journal of Mechanical Engineering and Technology. 8. 424-434.

BIBLIOGRAPHY:

[1] Benmessaoud, M., Nasreddine, M.M. Optimization of MEMS capacitive accelerometer. Microsyst Technol 19, 713–720 (2013). https://doi.org/10.1007/s00542-013-1741-z

[2] Z. Andrabi and K. A. Gupta, "Study and Analysis of Materials for Design of MEMS Capacitive Accelerometer," 2018 3rd IEEE International Conference on Recent Trends in Electronics, Information & Communication Technology (RTEICT), Bangalore, India, 2018, pp. 2183-2187, doi: 10.1109/RTEICT42901.2018.9012505.

[3] Z. Mohammed and M. Rasras, "Optimization of finger spacing and spring constant in comb type capacitive accelerometer," 2016 IEEE International Nanoelectronics Conference (INEC), Chengdu, 2016, pp. 1-2, doi: 10.1109/INEC.2016.7589291.

[4] Puccioni, Giulio. (2020). Design and Analysis of MEMS Capacitive Accelormeter.

[5] Niu, W. , Fang, L. , Xu, L. , Li, X. , Huo, R. , Guo, D. and Qi, Z. (2018) Summary of Research Status and Application of MEMS Accelerometers. Journal of Computer and Communications, 6, 215-221. doi: 10.4236/jcc.2018.612021.

[6] Vinay, P & Satya, Ch & Vamsi, Sri & Hemanth, M & Saiteja, A & Ali, .abid & Puli, Ashok & Satya, Venkata. (2017). Design and simulation of MEMS based accelerometer for crash detection and air bags deployment in automobiles. International Journal of Mechanical Engineering and Technology. 8. 424-434.

[7] J. Beitia, P. Loisel, C. Fell and I. M. Okon, "Miniature accelerometer for high-dynamic, precision guided systems," 2017 24th Saint Petersburg International Conference on Integrated Navigation Systems (ICINS), St. Petersburg, 2017, pp. 1-6, doi: 10.23919/ICINS.2017.7995641.

[8] Szermer, M. et al. "FEM analysis of a 3D model of a capacitive surface-micromachined accelerometer." 2017 14th International Conference The Experience of Designing and Application of CAD Systems in Microelectronics (CADSM) (2017): 432-434.

(This work is licensed under a Creative Commons Attribution 4.0 International License.)